

Biologically Activated Noble Metal Alloys at the Nanoscale: For Lithium Ion Battery Anodes

Yun Jung Lee,^{†,||} Youjin Lee,^{†,||} Dahyun Oh,[†] Tiffany Chen,[‡] Gerbrand Ceder,^{*,†} and Angela M. Belcher^{*,†,§}

[†] Department of Materials Science and Engineering, [‡] Department of Biology, and [§] Department of Biological Engineering, Massachusetts Institute of Technology, Cambridge, Massachusetts 02139

ABSTRACT We report the synthesis and electrochemical activity of gold and silver noble metals and their alloy nanowires using multiple virus clones as anode materials for lithium ion batteries. Using two clones, one for specificity (p8#9 virus) and one versatility (E4 virus), noble metal nanowires of high-aspect ratio with diameters below 50 nm were successfully synthesized with control over particle sizes, morphologies, and compositions. The biologically derived noble metal alloy nanowires showed electrochemical activities toward lithium even when the electrodes were prepared from bulk powder forms. The improvement in capacity retention was accomplished by alloy formation and surface stabilization. Although the cost of noble metals renders them a less ideal choice for lithium ion batteries, these noble metal/alloy nanowires serve as great model systems to study electrochemically induced transformation at the nanoscale. Given the demonstration of the electrochemical activity of noble metal alloy nanowires with various compositions, the M13 biological toolkit extended its utility for the study on the basic electrochemical property of materials.

KEYWORDS M13 virus, biomaterialization, alloy nanowire, energy storage, transformation at the nanoscale

The amount of energy stored in the lithium ion battery clearly depends on the cell's output potential and capacity, which are determined by the thermodynamics and chemistry of the system.¹ To minimize the reduction of cell voltage and thereby maximize the energy density, anode materials with very negative potential and high capacity have been searched for and studied. Metals or intermetallic compounds that can be alloyed with lithium are promising candidates due to the high theoretical capacity.^{2,3} Major challenges in these materials lie in the mechanical stress related to large volume changes and structural changes accompanied by lithium uptake and release. This mechanical stress results in pulverization and rapid capacity fading,⁴ which render these materials not very practical for prolonged usage. Among those materials capable of alloying with lithium, silver (Ag) and gold (Au) react with lithium at low voltage.⁵ Ag and Au form several alloy phases with lithium and can alloy with a very high percentage of Li (up to AgLi_9 and $\text{Au}_4\text{Li}_{15}$). However, little is known about the electrochemical response of Ag and Au with lithium. The available reports are mostly limited to thin film materials.^{5–8} When test electrodes were prepared by a normal fabrication process from powder, the capacity of Ag electrodes rapidly decays below 100 mAh/g within 10 cycles.²

Although a thin film material can mitigate the stress-related problems, the total energy stored in a thin film battery is not high enough for practical application due to the limited amount of materials in the thin film.

There is already prevailing evidence that nanostructured materials can improve the electrochemical properties of electrode materials compared to the bulk counterparts. One-dimensionally structured nanomaterials such as SnO_2 ⁹ and Si⁴ have shown improved performance as anodes for lithium ion batteries. In addition to excellent surface activity provided by the high surface-to-volume ratio, nanowires with small diameter can relieve mechanical stress associated with the large volume change upon lithiation, as well as reduce the distance over which Li needs to diffuse.

The inherent structural characteristic of the M13 virus makes this biological building block an excellent template for the synthesis of various functional nanowires with small diameter. The wild type filamentous M13 virus has a high aspect ratio with approximately a 6.5 nm diameter and an 880 nm length.¹⁰ Roughly 2700 copies of p8 coat protein self-assemble into the capsid of the wild-type virus, resulting in 5-fold symmetry along the length of virus. Computational simulation of M13 virus shows that the closest distance of p8 protein neighbors is around 3 nm.¹¹ In addition to these structural advantages, the functionality of subunit proteins of the M13 virus can be altered through genetic engineering. Previously, the virus has been engineered to display peptides that have affinity to specific target materials and used to bind, organize, and further nucleate those specific materials.^{11–13} For example, a gold-binding virus was se-

* To whom correspondence should be addressed. E-mail: (G.C.) gceder@mit.edu; (A.M.B.) belcher@mit.edu.

|| These authors contributed equally to this work.

Received for review: 02/18/2010

Published on Web: 05/27/2010

lected through an evolutionary screening process called biopanning. The M13 virus with a gold-binding peptide motif (VSGSSPDS) on the p8 major coat protein was named p8#9 and used for assembling gold nanoparticles.¹² In addition to the biomolecular recognition of specific materials identified through biopanning, the surface functionality of M13 virus can be modified independently through genetic engineering. The E4 virus is a modified M13 virus that has tetraglutamate (EEEE) fused to the amino terminus of each copy of the p8 major coat protein. Due to the presence of extra carboxylic acid groups compared with wild type M13 virus (M13KE), the E4 virus exhibited increased ionic interactions with cations and can serve as a template for materials growth. With this E4 virus, materials specificity was diminished, but versatility was enhanced. Our group reported successful nanowire synthesis of several functional materials such as Co_3O_4 ,¹⁴ amorphous FePO_4 ,¹⁵ and single crystalline Ag nanowires¹⁶ on the E4 templates. Here, we report the facile synthesis and improved electrochemical activity of noble metal and metal alloy nanowires using multiple virus clones for lithium ion battery anode materials.

In this work, we have synthesized nanowires of pure Ag and Au noble metals and their alloys with control over diameter, morphology, and composition using two independent M13 clones, one each for specificity (p8#9) and versatility (E4). The virus-enabled synthesis of noble metal nanowires was remarkably facile resulting in high-yield compared to the traditional methods for making noble metal nanomaterials.¹⁷ Synthesis of pure Ag nanowires was demonstrated in our previous work with E4 virus using spontaneous photoreduction.¹⁶ The spontaneous reduction produced straight single crystalline nanowires along the length of the virus, but the product yield was not high enough for practical application in bulk devices such as battery electrodes. The clone we used was termed E4. However, upon repeated rounds of amplification and followed by sequencing, the population of virus was determined to consist of mixture of three glutamate and four glutamate residues, so it is termed E3/E4. To increase Ag nanowire yield, a reducing agent, sodium borohydride (NaBH_4), was introduced. As seen in the transmission electron microscopy (TEM) image shown in Figure 1A, wavy polycrystalline Ag nanowires with rough surfaces were generated with the reduction with NaBH_4 . The nanowire size was estimated to be 15 nm in diameter. The different morphology could be associated with the increased nucleation sites from the NaBH_4 reduction, in contrast to the limited nucleation and specific growth on the seeds already formed in a self-catalyzed spontaneous reduction. The electrochemical properties of viral Ag nanowires were tested in the voltage window of 0–2.0 V against lithium foil in Figure 1C, which shows the first two discharge/charge curves. The viral Ag nanowires show pseudoplateaus at 0.08 and 0.02 V during the lithiation process while the removal of lithium from the alloy occurred in two steps at 0.14 and 0.3 V, which is in fairly good agreement with the previously reported

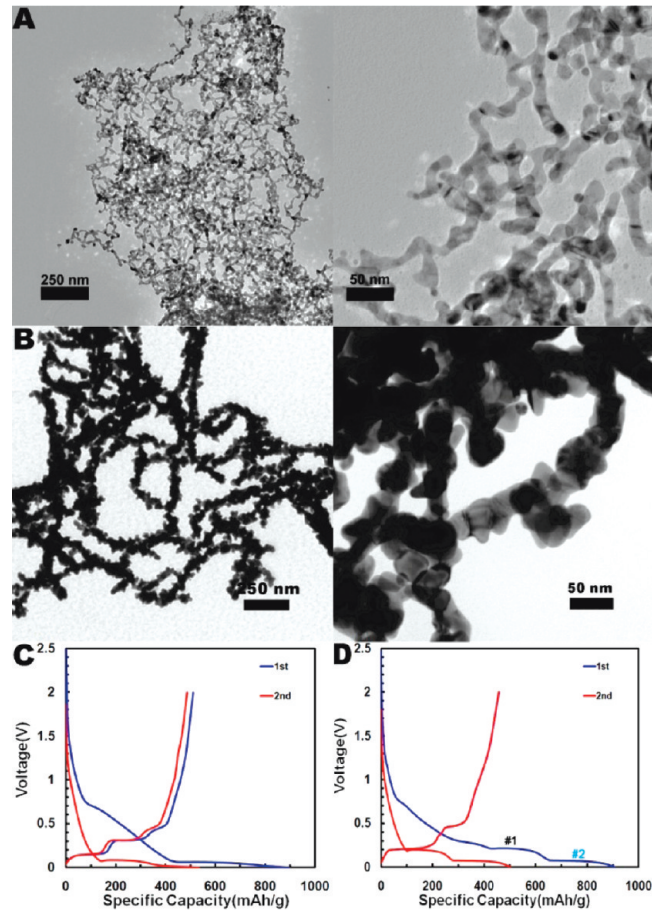


FIGURE 1. Characterization of surfactant-free pure Ag and pure Au viral nanowires. (A,B) TEM images of (A) Ag nanowires on E4/E3 virus and (B) Au nanowires on p8#9 virus; (C,D) First two discharge/charge curves tested between 0 and 2.0 V. (C) Ag nanowires on E4/E3 virus. Active material loading was $4.28 \text{ mg}/\text{cm}^2$. (D) Au nanowires on p8#9 virus. Active material loading was $5.55 \text{ mg}/\text{cm}^2$.

values.^{6,7} The plateaus in the potential profile stem from the two-phase coexistence regions in the phase diagrams. For a two-component system such as Ag–Li and Au–Li, Gibbs phase Rule determines the degree of freedom in a two-phase equilibrium regime as zero that renders the electrode potential independent of composition. While in principle all two-phase regions in the binary phase diagram should appear as plateaus,¹⁸ only two alloy phases have been reported to occur reversibly in the reaction with lithium.⁶ One unknown phase (designated as phase I)⁶ appeared during the first lithiation, however, this phase was still present at the end of the dealloying process and hence is considered irreversible. Unknown phase II⁶ was related to the plateaus at 0.08 V (alloying) and at 0.3 V (dealloying) and the $\text{AgLi}\beta$ phase was associated with the 0.02 V (alloying) and 0.14 V (dealloying) plateaus.⁶ In Figure 1C, a large irreversible capacity from 0.7 V down to the first alloying plateau appeared during the first discharge. The irreversible capacity in this voltage range was partly attributed to the formation of solid electrolyte interface (SEI) formation on the electrode surface with the decomposition of elec-

trolyte.^{19–22} The irreversible capacity also arises from the Super P carbon in the electrode. The irreversible capacity from Super P carbon was previously reported as ~600 mAh/g.²³ This capacity from Super P carbon was very irreversible and negligible in the following cycles. The viral silver nanowires delivered 534 mAh/g discharge capacity in the second cycle, which corresponds to the alloy composition of $\text{AgLi}_{2.15}$.

For the synthesis of pure Au nanowires, the p8#9 virus was selected for having a peptide motif expressed on the major coat protein with specific affinity to both gold ions and gold.¹² The specific gold binding sites on p8#9 not only attract the gold ions in the solution but also initiate the nucleation of spherical Au nanoparticles on the virus, so the final product was a collection of 5–7 nm Au nanoparticles along the M13 virus, rather than continuous nanowires. Therefore, we were not able to address the specific properties of Au with high aspect ratio from the previous method. To exploit the unique property of one-dimensional Au nanowires, the following criteria are required: homogeneous nanowires without small particles, uniform diameter along the length, and high nanowire yield from precursors. A stepwise reduction of Au^{3+} ions from the first partial reduction during the incubation for templating to the final reduction of Au^+ ions with mild reducing agent (ascorbic acid) resulted in Au nanowires with increasing the yield of continuous nanowires while decreasing the amount of extraneous free nanoparticles. Au^{3+} ions were introduced to the dilute aqueous p8#9 virus solution and the resultant mixture was incubated for half hour. During the incubation, the p8#9 virus attracts Au^{3+} ions in the solution and also partially reduces Au^{3+} ions to Au^+ simultaneously. The growth of Au nanowires was completed by the addition of reducing agent at an elevated temperature to get continuous nanowire structures. In Figure 1B, pure Au nanowires with diameter around 40 nm demonstrated rough surfaces, which can be smoothened either by the addition of silver ions and surfactants as will be described later.

The electrochemical response of viral Au nanowires with lithium was examined in the voltage range of 0–2.0 V (measured against metallic Li) (Figure 1D). Well-defined plateaus were observed at 0.2 and 0.1 V during alloying with lithium and at 0.2 and 0.45 V during the dealloying process. These values are in good agreement with the limited number of reported values.^{3,5,8} A large irreversible capacity was also observed between 0.7 and 0.2 V. The specific discharge capacity was 501 mAh/g at the second cycle, which corresponds to the alloy composition of $\text{AuLi}_{3.69}$.

To investigate the effect of noble metal alloying on the lithiation behavior, Au–Ag alloy nanowires with controlled composition were produced on p8#9. Because of the Au-specificity in the p8#9 virus, preparation of Au–Ag alloy nanowires with homogeneous composition without any segregation of single atom was done without difficulty. However, the addition of Ag atoms not only increased the Ag contents in the alloy nanowires but also reduced the

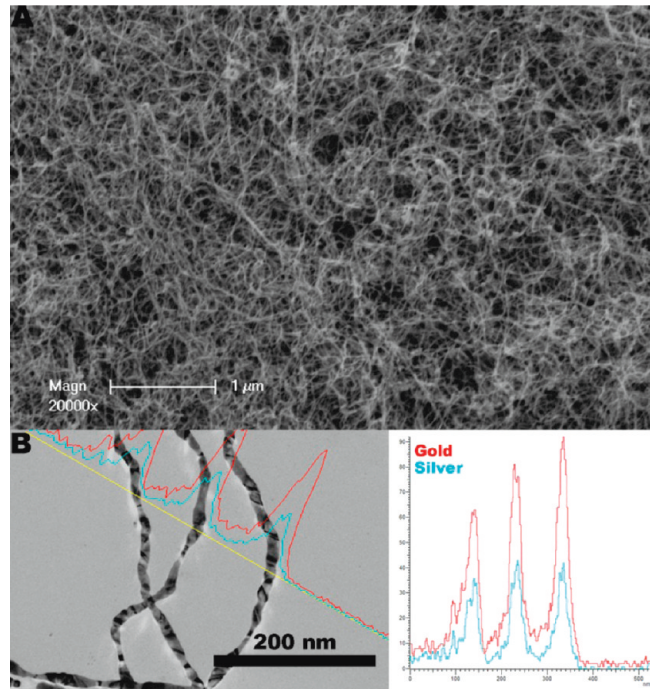


FIGURE 2. Structural characterization of CTAB-stabilized $\text{Au}_x\text{Ag}_{1-x}$ alloy nanowires on p8#9 virus. (A) SEM images of $\text{Au}_{0.67}\text{Ag}_{0.33}$ nanowires (B) TEM-EDX line scanning exhibits the presence of two elements Au and Ag in the template nanowires.

roughness of the nanowires by reducing the branched structures observed in pure viral Au nanowires. To create a well-developed surface regardless of the Ag contents in the alloy nanowires, cetyl trimethylammonium bromide (CTAB), a water-soluble and M13 compatible surfactant molecule, was introduced. In this surfactant-mediated biomineralization of Au–Ag alloy nanowires, higher concentration of p8#9 was introduced to the CTAB solution resulting in surfactant-coated p8#9. Because of the strong specific interaction between Au^{3+} ions and p8#9, Au^{3+} ions penetrated the surfactant layer and successfully templated through the extended incubation time up to three hours. As in the synthesis of pure Au nanowires, the partial reduction of yellow Au^{3+} ions to colorless Au^+ ions occurred during the incubation, and the formation of alloy nanowires was completed by the addition of ascorbic acid and silver ions sequentially.

In Figure 2A, a porous network of smooth and uniform nanowires is visualized using scanning electron microscopy (SEM). A TEM-energy dispersive X-ray spectroscopy (TEM-EDX) line scan in Figure 2B clearly verified the formation of $\text{Au}_x\text{Ag}_{1-x}$ alloy, and quantitative EDX analysis determined the Au/Ag ratio as 2:1 for the nanowires in this image. This composition was also confirmed by inductively coupled plasma optical emission spectroscopy (ICP-OES) after two days of digestion in aqua regia. EDX point analysis of the same nanowires confirmed that the nanowires have uniform homogeneous composition. On the other hand, the nanowires grown on the wild-type M13 virus showed nonuniform

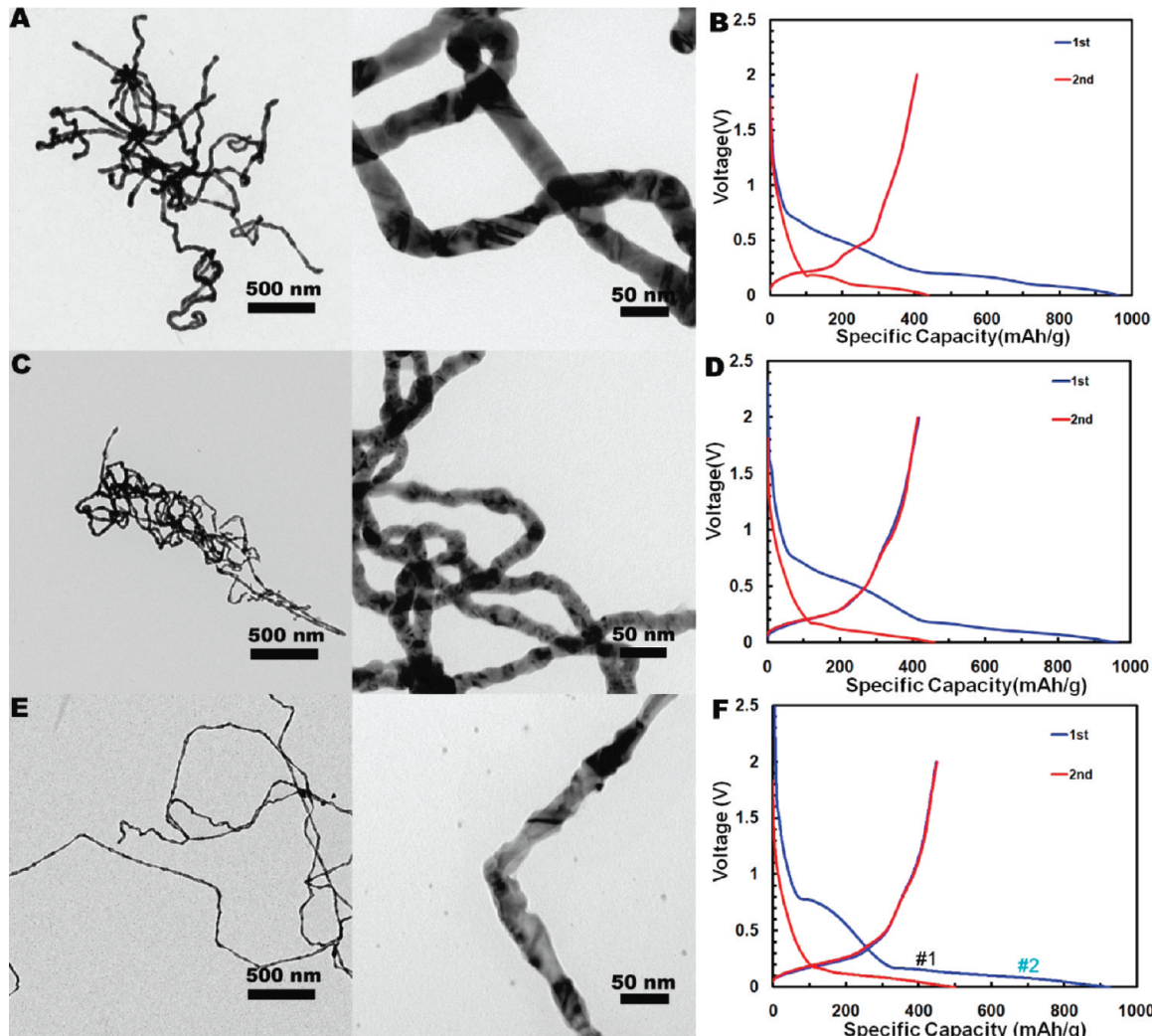


FIGURE 3. Characterization CTAB-stabilized $\text{Au}_x\text{Ag}_{1-x}$ alloy nanowires on p8#9 virus. (A,B) $\text{Au}_{0.9}\text{Ag}_{0.1}$ nanowires. (A) TEM images. (B) First two discharge/charge curves tested between 0 and 2.0 V with active material loading 5.11 mg/cm^2 . (C,D) $\text{Au}_{0.67}\text{Ag}_{0.33}$ nanowires. (C) TEM images. (D) First two discharge/charge curves tested between 0 and 2.0 V with active material loading 4.47 mg/cm^2 . (E,F) $\text{Au}_{0.5}\text{Ag}_{0.5}$ nanowires. (E) TEM images. (F) First two discharge/charge curves tested between 0 and 2.0 V with active material loading 3.89 mg/cm^2 .

composition along the virus even though the average composition was the same as the nanowires grown on the p8#9 virus. TEM images in Figure 3A,C,E also showed homogeneous nanowires of uniform diameter without the side product. Compared with the nanowires with free surfaces shown in Figure 1, the nanowires prepared from the surfactant-mediated method have the advantage of having more uniform diameter and reduced aggregation between nanowires. We assume that these morphological changes are related to the addition of CTAB surfactant, which serves as a surface stabilizer reducing surface energies, and thus can enhance the uniformity of surface morphology.

To explore how the degree of alloying (composition) affects the lithiation process, alloy nanowires with three different compositions were prepared and tested in a Li cell, $\text{Au}_{0.5}\text{Ag}_{0.5}$, $\text{Au}_{0.67}\text{Ag}_{0.33}$, and $\text{Au}_{0.9}\text{Ag}_{0.1}$. Compositions were determined from quantitative TEM-EDX analysis and ICP-OES. The diameters of the nanowires are 25 nm for

$\text{Au}_{0.5}\text{Ag}_{0.5}$, 20 nm for $\text{Au}_{0.67}\text{Ag}_{0.33}$, and 30 nm for $\text{Au}_{0.9}\text{Ag}_{0.1}$ (Figure 3A,C,E). The galvanostatic response of the $\text{Au}_x\text{Ag}_{1-x}$ alloy nanowires did not show discrete plateaus but gradual changes in potential from 0.2 to 0 V during discharge, and from 0 to 0.5 V during charge, indicative of a single-phase evolution. (Figure 3B,D,F). However, as the Au composition increases close to 1, the potential profile starts to resemble that of pure Au.

To find out the alloy phases that form in the electrochemical lithiation process, XRD patterns were obtained at different stages of Li-alloying for pure Au and $\text{Au}_{0.5}\text{Ag}_{0.5}$ nanowires (Figure 4). Since the potential profile of Au with Li is strikingly similar to the one for Ag–Li (except for the absolute values of the plateau potentials), and Au and Ag have the same crystal structure, we consider that similar alloy structures may form, including phase II and the β phase (AuLi , in this case) during the lithiation process. The B2-structured β phase is common to both the Au–Li and Ag–Li phase diagram. In

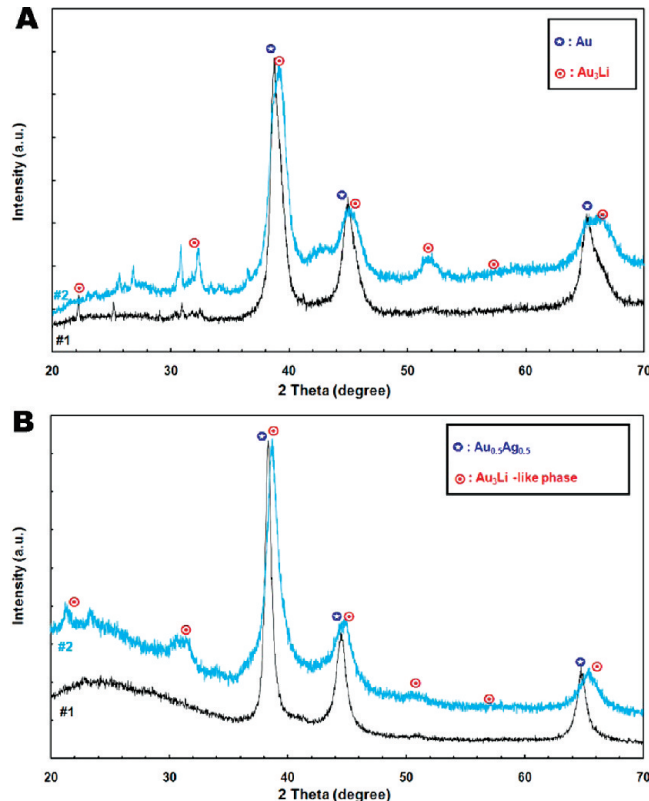


FIGURE 4. XRD evolution patterns at different stages of alloying process. Stage #1 and #2 are denoted in Figure 1D and Figure 3F. (A) Pure Au nanowires and (B) Au_{0.5}Ag_{0.5} nanowires.

Figure 4A, Au and ordered Au₃Li α_1 phases were identified at stage #1 of the 0.2 V discharge plateau. (Refer to Figure 1D for the position of stage #1 and #2.) At stage #2 of the 0.1 V plateau, peak intensities from Au₃Li α_1 phase were increased while the intensity of peaks from Au was decreased. No obvious formation of AuLi β phase was observed. For the Au_{0.5}Ag_{0.5} alloy nanowires, only a single peak can be observed at stage #1 indicating that lithium was incorporated into a single phase of Au_{0.5}Ag_{0.5}. (Refer to Figure 3F for the position of stage #1 and #2.) The peaks at stage #2 were indexed as an Au₃Li-like α_1 phase with a small amount of the initial-Au_{0.5}Ag_{0.5}-like phase. Since the (Au_{0.5}Ag_{0.5})₃Li α_1 phase has not been previously reported, further chemical composition analysis is required to identify the exact phase.

The electrochemical responses of Au_xAg_{1-x} alloy nanowires for different x are compared in Figure 5. This comparison clearly shows that while Ag and Au react with significant voltage plateaus, the alloys present gradual changes in the potential profile with lithiation. In particular the Au_{0.5}Ag_{0.5} material shows pseudosingle phase behavior with lithium. The single-phase like potential profile can arise for several reasons. If Ag and Au cannot separate on the time-scale of the lithiation, the starting material essentially acts like a single component material with substantial disorder. The substitutional disorder of Au and Ag creates locally

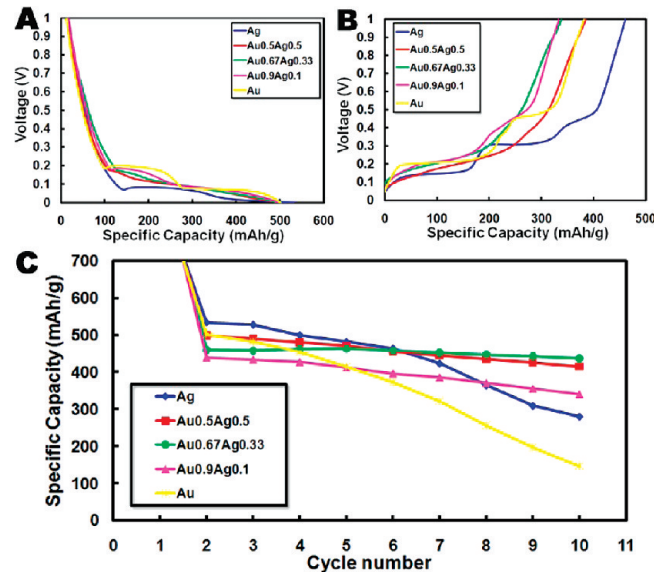


FIGURE 5. Electrochemical properties of Au_xAg_{1-x} alloy nanowires with composition ($x = 1, 0.9, 0.67, 0.5$, and 0) tested between 0 and 2.0 V. (A) Second discharge curves, (B) second charge curves, and (C) capacity retention for 10 cycles.

varying site energies for lithium resulting in a changing potential as lithiation proceeds. Hence, such a “disordered” system acts as a single phase when lithiated with no discrete phase transitions. However, even the formation of two phases upon lithiation does not necessarily imply that the potential should be constant. If Au and Ag are mobile enough to partition between the two phases, the system can be considered a ternary with respect to the Gibbs phase Rule and coexistence of two phases (host Au_xAg_{1-x} and ternary alloys of Au–Ag–Li) leaves one degree of freedom (Gibbs phase Rule at constant temperature and pressure, $F = C - P = 3 - 2 = 1$). Therefore the potential can be dependent on the Li content. Note that this argument becomes invalid if the kinetics of Au and Ag is so slow that they would not be able to redistribute. In that case, no equilibrium condition can be applied for the Au and Ag distribution and the system will act as a pseudo binary.

As the Au content increases in Au_xAg_{1-x} alloys, the discharge/charge potentials increase. The discharge/charge potentials were clearly dependent on the composition. Since the potential is determined by thermodynamics, the activity of Li in the materials could be changed in the homogeneous alloy structure having values dependent on the composition. The first discharge capacity of all the alloys were all similar with values 900–965 mAh/g, but because of the high first cycle irreversible capacity, the second discharge capacities dropped to 440–534 mAh/g depending on the alloy composition. For most Ag and Au thin film anodes, the discharge capacity was previously reported as 500–600 mAh/g at the first cycle and decreased to 100–200 mAh/g in 10 cycles.^{8,24} The best reported Ag thin film maintained 520 mAh/g for 10 cycles.^{6,7} When a Ag electrode was prepared from bulk

powder forms, the discharge capacity faded rapidly and dropped below 50 mAh/g in 10 cycles.² In Figure 5C, the capacity retention of the viral pure Ag, Au, and alloy nanowires for 10 cycles is shown. While the pure, surfactant-free Au and Ag nanowires show rapid capacity fading, the alloys display improved capacity retention. There have been several reports that some alloys that make an active/inactive composite structure with lithium can improve cycling performance due to the buffering effect of the inactive component.²⁵ Other alloys that have components both active with lithium displayed stable capacity retention when the components make intermetallic compounds that have little/moderate volume changes when alloyed with lithium.² Since both Au and Ag are able to alloy with lithium and their alloys have the same structure as Au and Ag, the improvement in our Au–Ag alloy system cannot be explained with the reasons listed above. Instead, we speculate that the improvement of capacity retention in our alloy system is associated with CTAB surface stabilization and/or the pseudosingle phase behavior in potential profiles. To demonstrate how the surface stabilization and alloy formation affect the electrochemical performance of noble metal alloys, $\text{Au}_{0.9}\text{Ag}_{0.1}$ and $\text{Au}_{0.5}\text{Ag}_{0.5}$ nanowires were synthesized without CTAB surfactants. We excluded the contribution of CTAB to the capacity because the content of remaining CTAB after ethanol washing was determined to be only 2 wt % from thermogravimetric analysis (TGA) results, and the electrochemical response of CTAB with lithium in the testing voltage window (Supporting Information, Figure S2) was negligible. In Figure 6A, surfactant-free $\text{Au}_{0.9}\text{Ag}_{0.1}$ nanowires with an average 35 nm in diameter having rough surface were templated on the virus. The electrochemical responses in the first three galvanostatic cycles from the two nanowires with different surfaces were almost identical with slightly different specific capacities (Supporting Information, Figure S1A). However, as shown in Figure 6B, capacity retention for 10 cycles shows a clear difference. The specific capacity of surfactant-free nanowires decreased rapidly within 10 cycles, while that of nanowires with CTAB-stabilized surface showed rather moderate fading. For the nanowires with CTAB-stabilized surface, particle-coalescence upon cycling could be suppressed due to the presence of the surface-adsorbed CTAB. More importantly, nanowires grown without CTAB are more branched and thus could experience more homogenizing force by Oswald ripening, which leads to poor cycling performance. One might argue that the different number of virus templates is the reason for better cycling performance for the CTAB-stabilized alloys, since the virus-to-metal ratio is higher (about 5 times) for CTAB-stabilized alloys than for surfactant-free ones (Supporting Information). When surfactant-free nanowires with the [virus]/[metal] ratios as high as CTAB-stabilized ones were synthesized and tested, there was no significant change in the cycling performance thereby ruling out the possible template effect in the experimental condition used here (Supporting

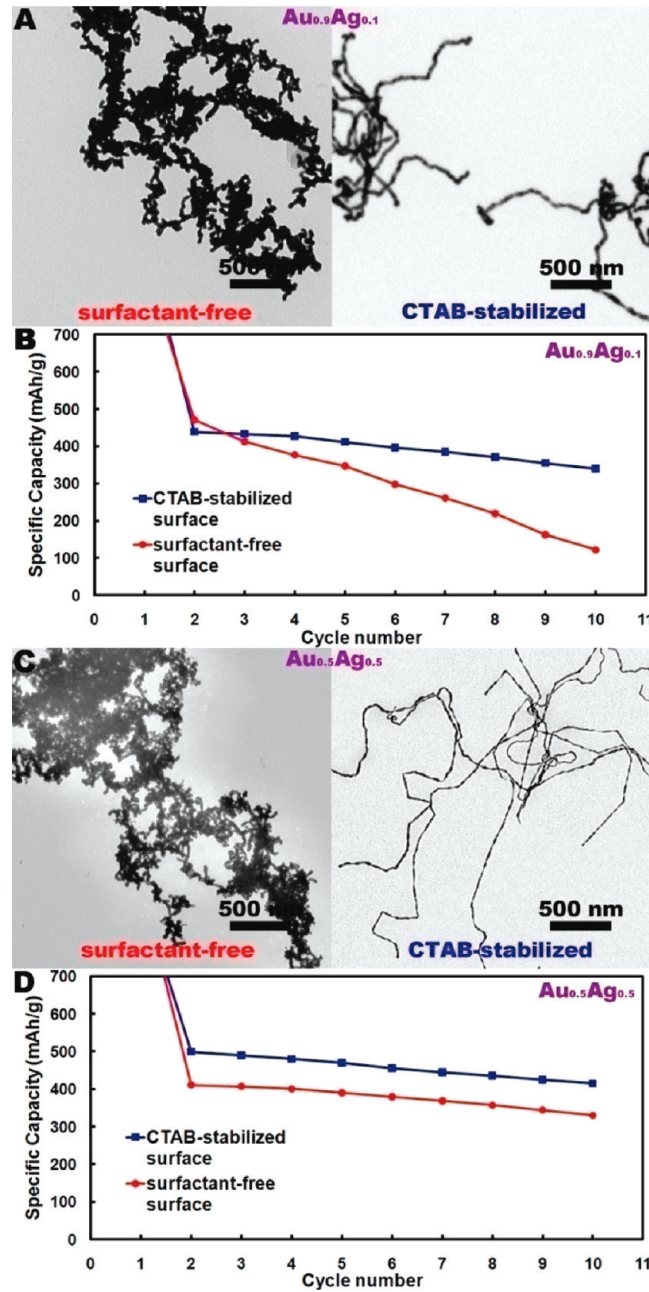


FIGURE 6. Effect of surface stabilization and alloy formation on the capacity retention. Comparison of nanowires with same compositions but different surfaces (surfactant-free vs CTAB stabilized). (A,B) $\text{Au}_{0.9}\text{Ag}_{0.1}$ nanowires with (A) morphology (TEM images) and (B) capacity retention for 10 cycles. (C,D) $\text{Au}_{0.5}\text{Ag}_{0.5}$ nanowires with (C) morphology (TEM images) and (D) capacity retention for 10 cycles.

Information). Although CTAB stabilization can improve cycling performances, there can be another explanation for the better capacity retention for the $\text{Au}_x\text{Ag}_{1-x}$ alloy nanowires. Strain in a material depends not on the overall volume change of the lithiation reaction but on the inhomogeneity of that volume change. Two-phase reactions are inherently inhomogeneous with a reaction front separating both phases. Similarly, poor diffusion kinetics can lead to concentration

TABLE 1. Summary of Second and Tenth Discharge Capacities for Various Viral Nanowires Tested

	materials		capacities (mAh/g)	
	composition	size (diameter)	second cycle	tenth cycle
surfactant-free	Au	40 nm	502	146
	$\text{Au}_{0.9}\text{Ag}_{0.1}$	35 nm	471	122
	$\text{Au}_{0.5}\text{Ag}_{0.5}$	30 nm	411	330
	Ag	15 nm	534	280
CTAB- stabilized	$\text{Au}_{0.9}\text{Ag}_{0.1}$	30 nm	439	340
	$\text{Au}_{0.67}\text{Ag}_{0.33}$	20 nm	459	437
	$\text{Au}_{0.5}\text{Ag}_{0.5}$	25 nm	499	415

gradients and hence inhomogeneous volume change. These inhomogeneities caused by direct lithium gradients in two-phase coexistence are believed to be one of the reasons for poor capacity retention.²⁶ In terms of reaction homogeneity, the pseudosingle phase behavior in the potential profile for $\text{Au}_x\text{Ag}_{1-x}$ alloys can therefore be beneficial. However, it is difficult to tell in this study if both homogeneity and surface stabilization are relevant or if only one of them is relevant for the better cycling performance. To clearly check the importance of surface stabilization and reaction homogeneity, surfactant-free $\text{Au}_{0.5}\text{Ag}_{0.5}$ alloy nanowires were also investigated. The potential profiles of the two $\text{Au}_{0.5}\text{Ag}_{0.5}$ alloy nanowires with different surfaces were almost identical but the surfactant-free one displayed lower specific capacity (Supporting Information, Figure S1B). Contrary to the gold-rich $\text{Au}_{0.9}\text{Ag}_{0.1}$ alloy, the capacity retention for 10 cycles was similar for both CTAB-stabilized and surfactant-free nanowires for $\text{Au}_{0.5}\text{Ag}_{0.5}$ alloy (Figure 6D). The specific capacity was moderately stable for 10 cycles for both nanowires. This result implies that the capacity retention can be improved by forming alloys with composition close to $\text{Au}/\text{Ag} = 1:1$ even without surface stabilization. However, for an $\text{Au}_{0.9}\text{Ag}_{0.1}$ alloy that is less alloyed and more close to pure Au, surface characteristics dominate capacity retention. Reducing the material dimension proved to be effective in decreasing mechanical stress, however, other factors such as homogeneity and surface stabilization appeared more influencing for the nanowires with diameter below 50 nm in this study based on capacity retention of pure Ag nanowires. Surfactant-free pure Ag nanowires with rough surface showed poor cycling performance even with the smallest particle size among the tested nanowires (15–20 nm). To numerically show the importance of surface stabilization and alloy formation, the second and tenth discharge capacities and diameters for various viral nanowires tested are summarized in Table 1. Although the alloy nanowires with diameters below 30 nm showed moderate improvement in cycling performance up to 10 cycles, all alloy nanowires eventually failed to maintain stable capacity when tested up to 20 cycles. Further designing alloy nanostructures on the virus template to suppress coalescence is under investigation for better cycling performance.

Biological systems offer capabilities for environmentally benign materials synthesis. The two M13 viruses, genetically

engineered for specificity (p8#9 virus) and versatility (E4/E3 virus) served as a template for the synthesis of noble metal nanowires with diameters below 50 nm. The inherent structural characteristic of the M13 virus enabled the synthesis of high aspect ratio nanowires. With the synergistic combination of biological building blocks and synthetic chemistry, this facile and high-yield synthesis conferred controls over particle size, morphology, and compositions. The biologically derived noble metal and alloy nanowires with diameter below 50 nm showed electrochemical activities toward lithium comparable to thin film electrodes. Improvement in capacity retention was achieved by tailoring particle size, alloy formation, and surface stabilization. Because Au and Ag react poorly with lithium at the micrometer scale, fundamental study on their electrochemical behavior has been limited so far. Although these materials are not as cost-effective as existing anode materials, these nanowires serve as a model system in identifying important parameters that can induce stable electrochemical transformation at the nanoscale. This study elucidated the importance of surface characteristics and reaction/phase homogeneity in maintaining structural stability and electrochemical performances at the nanoscale. The principles found in this model system can be applied to improve structural stability of other technologically important alloy material systems. With advantages of facile and environmentally benign synthesis, M13 biological platform proved itself as a useful toolkit for the study on the basic electrochemical property of materials.

Acknowledgment. This work was supported by the Army Research Office Institute of the Institute of Collaborative Biotechnologies (ICB) and U.S. National Science Foundation through the Materials Research Science and Engineering Centers program. Y.L. acknowledges a Samsung Scholarship from Samsung Foundation of Culture and D.O. is grateful for Kwanjeong foundation for a scholarship. The authors would like to thank Dong Soo Yun for assistance analyzing the alloy materials with the TEM-EDX and Yoon Sung Nam for imaging nanowires with SEM.

Supporting Information Available. Materials and Methods, Figures S1 and S2. Figure S1 is the third discharge/charge curves of $\text{Au}_{0.9}\text{Ag}_{0.1}$ nanowires and $\text{Au}_{0.5}\text{Ag}_{0.5}$ nanowires with different surface stabilization but at the same composition. Figure S2 is the galvanostatic data of CTAB. This material is available free of charge via the Internet at <http://pubs.acs.org>.

REFERENCES AND NOTES

- Armand, M.; Tarascon, J. M. *Nature* **2008**, *451*, 652–657.
- Yin, J. T.; Wada, M.; Yoshida, S.; Ishihara, K.; Tanase, S.; Sakai, T. *J. Electrochem. Soc.* **2003**, *150*, A1129–A1135.
- Laik, B.; Eude, L.; Pereira-Ramos, J. P.; Cojocaru, C. S.; Pribat, D.; Rouviere, E. *Electrochim. Acta* **2008**, *53*, 5528–5532.
- Chan, C. K.; Peng, H. L.; Liu, G.; McIlwrath, K.; Zhang, X. F.; Huggins, R. A.; Cui, Y. *Nat. Nanotechnol.* **2008**, *3*, 31–35.
- Taillasses, G.; Benjelloun, N.; Sarradin, J.; Ribes, M. *Solid State Ionics* **2002**, *152*, 119–124.

- (6) Taillades, G.; Sarradin, J. *J. Power Sources* **2004**, *125*, 199–205.
- (7) Morales, J.; Sanchez, L.; Martin, F.; Ramos-Barrado, J. R.; Sanchez, M. *J. Electrochem. Soc.* **2004**, *151*, A151–A157.
- (8) Yuan, L.; Liu, H. K.; Maaroof, A.; Konstantinov, K.; Liu, J.; Cortie, M. *J. New Mater. Electrochem. Syst.* **2007**, *10*, 95–99.
- (9) Park, M. S.; Wang, G. X.; Kang, Y. M.; Wexler, D.; Dou, S. X.; Liu, H. K. *Angew. Chem., Int. Ed.* **2007**, *46*, 750–753.
- (10) Kay, B. K.; Winter, J.; McCafferty, J. *Phage Display of Peptides and Proteins: A Laboratory Manual*; Academic Press Inc.: San Diego, CA, 1996.
- (11) Mao, C. B.; Solis, D. J.; Reiss, B. D.; Kottmann, S. T.; Sweeney, R. Y.; Hayhurst, A.; Georgiou, G.; Iverson, B.; Belcher, A. M. *Science* **2004**, *303*, 213–217.
- (12) Huang, Y.; Chiang, C. Y.; Lee, S. K.; Gao, Y.; Hu, E. L.; De Yoreo, J.; Belcher, A. M. *Nano Lett.* **2005**, *5*, 1429–1434.
- (13) Lee, S. K.; Yun, D. S.; Belcher, A. M. *Biomacromolecules* **2006**, *7*, 14–17.
- (14) Nam, K. T.; Kim, D. W.; Yoo, P. J.; Chiang, C. Y.; Meethong, N.; Hammond, P. T.; Chiang, Y. M.; Belcher, A. M. *Science* **2006**, *312*, 885–888.
- (15) Lee, Y. J.; Yi, H.; Kim, W. J.; Kang, K.; Yun, D. S.; Strano, M. S.; Ceder, G.; Belcher, A. M. *Science* **2009**, *324*, 1051–1055.
- (16) Nam, K. T.; Lee, Y. J.; Krauland, E. M.; Kottmann, S. T.; Belcher, A. M. *ACS Nano* **2008**, *2*, 1480–1486.
- (17) Lee, Y.; Kim, J. H.; Yun, D. S.; Nam, Y. S.; Oi, J.; Gasteiger, H. A.; Yang, S. H.; Belcher, A. M. Submitted for publication.
- (18) Huggins, R. A. *J. Power Sources* **1999**, *81*, 13–19.
- (19) Aurbach, D.; Markovsky, B.; Levi, M. D.; Levi, E.; Schechter, A.; Moshkovich, M.; Cohen, Y. *J. Power Sources* **1999**, *81*, 95–111.
- (20) Hassoun, J.; Derrien, G.; Panero, S.; Scrosati, B. *Adv. Mater.* **2008**, *20*, 3169–3175.
- (21) Kim, H.; Cho, J. *Nano Lett.* **2008**, *8*, 3688–3691.
- (22) Yang, X. L.; Wen, Z. Y.; Xu, X. X.; Lin, B.; Lin, Z. X. *J. Electrochem. Soc.* **2006**, *153*, A1341–A1344.
- (23) Gómez Cámera, J. L.; Morales, J.; Sánchez, L.; Ruchb, P.; Ng, S. H.; Kötz, R.; Novák, P. *Electrochim. Acta* **2009**, *54*, 6713–6717.
- (24) Xue, M. Z.; Cheng, S. C.; Yao, J.; Fu, Z. W. *Electrochim. Acta* **2006**, *51*, 3287–3291.
- (25) Idota, Y.; Kubota, T.; Matsufuji, A.; Maekawa, Y.; Miyasaka, T. *Science* **1997**, *276*, 1395–1397.
- (26) Kwon, Y.; Kim, H.; Doo, S. G.; Cho, J. H. *Chem. Mater.* **2007**, *19*, 982–986.